Heliyon 10 (2024) e24064

Contents lists available at ScienceDirect

Heliyon

journal homepage: www.cell.com/heliyon

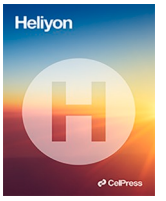

Research article

# Process modeling and simulation of *Gmelina arborea* (GmW) and *Mansonia altissima* (MaW) wood drying

C. Ajike, S.O. Enibe, U.C. Okonkwo, J.L. Chukwuneke *

*Department of Mechanical Engineering, Nnamdi Azikiwe University, Awka, Nigeria*

ARTICLE INFO

*Keywords:*
Drying
Moisture desorption isotherm
Thin-layer kinetic model
Gmelina arborea
Mansonia altissima
Wood

ABSTRACT

This study simulate the process modeling of drying characteristics of *Gmelina arborea* (GmW) and *Mansonia altissima* (MaW) wood under the influence of various process variables such as drying time, drying temperature, and airflow velocity. GmW and MaW moisture desorption isotherms, kinetics, and thermodynamics were also studied. Five (5) thin-layer and desorption isotherm drying models were used to model the moisture ratio and water activity data from the process. According to the anatomical analysis, the GmW sample has an average lumen size of 147.44 m, indicating a high moisture content. The results showed that the Guggenheim, Anderson, and de Boer (GAB) model with the lowest sum of squared error value (0.046) demonstrated the best-fit to the experimental desorption data for GmW samples and the Henderson-P model for MaW samples, while the Demir et al. model emerged as the best kinetics model fit for describing the moisture desorption isotherm and thin-layer drying kinetics. GmW effective diffusivity (Deff) values ranged from $3.671 \times 10^{-8}$ to $5.378 \times 10^{-8}$ $m^2/s$ and MaW effective diffusivity (Deff) values ranged from $2.923 \times 10^{-8}$ to $4.678 \times 10^{-8}$ $m^2/s$. GmW and MaW activation energies were 252.702 kJ/mol and 313.604 kJ/mol, respectively. The thermodynamic studies revealed that the heat and mass transfer coefficients varied linearly with temperature, as the change in enthalpy (ΔH) and change in entropy (ΔS) decreased while the Gibbs free energy (ΔG) increased. The results obtained from this study demonstrated that the proposed drying process modeling and simulation approach could be successfully applied to investigate the wood drying phenomena. The information can be used to reduce the drying costs and improve the wood quality.

## 1. Introduction

Wood and its byproducts are critical to civilization and human development all over the world. In Nigeria, for instance, wood, as a forest resource, contributes significantly to the Gross National Product (GNP) [1]. Similarly, as a renewable resource, wood frequently serves the dual purpose of being both an energy source and a fundamental raw material in the construction industry [2,3]. Because of its unique specific strength and aesthetic quality, it is also useful for artistic purposes [4,5]. Following a surge in infrastructure development, there is an increasing trend in wood harvesting, and it has been well established that trees have a high moisture content that contributes to their functional make-up [6,7]; Argo & Ubaidilla, 2020; [8]. As a result, freshly cut lumber has high moisture content, as expected. The lumbering industry has suffered significant economic losses and waste as a result of a lack of commensurate effort toward effective post-harvest processing. To address these concerns, the shelf life and suitability of harvested timbers (for many

* Corresponding author.
*E-mail address:* jl.chukwuneke@unizik.edu.ng (J.L. Chukwuneke).

https://doi.org/10.1016/j.heliyon.2024.e24064
Received 23 June 2023; Received in revised form 2 January 2024; Accepted 3 January 2024
Available online 6 January 2024

of their various applications) should be increased by removing excess moisture through seasoning [8,9]. Drying is an important part of wood seasoning and preparing it for further use in the construction industry. The vast majority of harvested woods, however, are left to dry in an uncontrolled interactive environment. Such a drying method results in slow moisture loss and rapid deterioration of lumber quality [10,11].

The concept of effective wood drying using artificial kilns has come to the forefront as a result of intense efforts to understand the drying process and the associated mechanisms. Drying operations using artificial dryers are quick and allow uniform moisture loss [12]. According to Ref. [13]; when drying is done properly, the dimensions of the wood remain stable, while the incidences of biological degradation/fungal infestation are significantly reduced. Some researchers have published papers, the majority of which concern the drying of food products [14]. investigated tomato thin-layer drying kinetics in a pilot-scale convective dryer by fitting experimental data into nine (9) different thin-layer drying models. [15]; effectively described the model in the tomato drying curve based on the high coefficient of determination and low error values (reduced sum of the square, SSE, and root mean square error, RMSE). The thin-layer drying properties of bamboo slices dried on a convective tray dryer were studied [16]. Fitting the experimental data into four (4) drying models revealed that the Page and logarithmic models had the highest coefficient of determination values ($R^2$) and the lowest RMSE at all temperatures, providing a better description of the drying mechanism [17]. reported on the thin-layer drying behavior of tomatoes and its mathematical modeling. According to the results, the GAB model was the best descriptive desorption isotherm, while the drying curves only showed the preheating and falling drying rate periods.

This work is justified in the absence of a substantial literature report on the drying of lumbers in general and MaW samples in particular. According to the literature, understanding the fundamentals and unique drying characteristics of a given material requires efficient application and analysis of thin-layer models [18,19]. The findings of such studies can also be used to simulate a wide range of drying operations and quantify the relevant design parameters for specialized drying equipment. Several thin-layer mathematical models have been developed and are classified into three types: theoretical, semi-theoretical, and fully empirical [20]. The semi-theoretical models are the focus of this study because they relate to the external resistance and moisture transfer between drying materials and air [21]. Similarly, the moisture sorption isotherm (MSI) captures the relationship between water activity, moisture content, and temperature. The use of several MSI for determining sorption isotherms, as well as the effects of thermodynamic and process variables on the GmW and MaW drying processes, are also discussed in this study.

The general desirability of GmW and MaW wood species in the Nigeria timber industry occasioned by the combined effects of its fast growth, strength, and relative ease of moisture desorption has been reported [22]; Inyang et al., 2018; [23,24]. Despite the fact that these woods are highly sought-after, an extensive literature survey portrayed the existence of few reports on their mathematical modeling, drying kinetics, moisture desorption isotherm modeling, and thermodynamic properties which hold great information on their (GmW and MaW wood species) large scale drying application. In order to stem the tide, this study sought to investigate and understand all aspects of wood drying process parameters which has been identified as critical to drying and wood products finishing thereby carving a niche in this area of study. Furthermore, attention was directed at modeling and simulating the drying process parameters of GmW and MaW wood species.

## 2. Materials and methods

### 2.1. Material collection and preparation

The unprocessed GmW and MaW used in the study were obtained from a local sawmill in Edo State, Nigeria (Lat. 6.5438°N and Long. 5.8987°E). Visual inspection was used to categorize the physical properties of the wood sample. The feel-and-touch method was used to determine the composition of the wood grain texture.

### 2.2. Anatomical investigation

Wood samples of the specified size (0.01 × 0.01 m) were obtained and boiled in water for 2 h to soften and drive out trapped air. The samples were then cut into transverse, radial, and longitudinal sections with a Reichert sliding microtome (model 843-02 G) and washed in distilled water. Sections of the samples were stained in safranin for 2 min to prepare them for microscopic examination and then washed with distilled water to remove the safranin stains. Following washing, the sections were tinkered with by dipping them in various ethanol concentrations (5 %–50 %) to reduce the risk of damage. Following that, the wood sections were treated with clove oil for 1 h to remove any remaining traces of ethanol from the specimen. Excess clove oil was removed from the samples using filter paper before mounting them on a slide. Slight Canada balsam was added as a mounting medium for preservation, and the slide was covered again with glass. Colouring materials that could impair visibility under the microscope were bleached away by immersing the specimen in 5 % sodium hydroxide (NaOH) for about 30 min. The specimen was then soaked in sodium hypochlorite (NaOCl) for 24 h and rinsed several times in water, while air bubbles were removed with gentle heat. Following that, a colored photomicrograph of the samples was taken with the Reichert light microscope's digital camera. The parameters studied in this research work included lumen size, fibre length, fibre diameter, density and ray width of Gmelina arborea and Mansoniaaltissima. The above-mentioned descriptive terminologies, measurements, and microscopic features for hardwood identification are all consistent with [25].

### 2.3. Wood seasoning experimentation

The freshly sawn samples were loaded into the Laboratory-scale wood-drying machine (LSWDM) with dimensions of 0.5 m × 0.25

m x 0.0254 m. The device was made of a stainless steel sheet and insulated from the elements with a 0.0254 m loose-fill thermal fiberglass insulator. To ensure even and adequate air circulation, the specified number of wood samples (about 10 samples of the aforementioned dimension per batch) was piled into the LSWDM while leaving about a 0.0254 m separation gap. The system was run in a closed-loop mode, with the fan producing unidirectional airflow.

An electric 0.6 kW heater at the inlet duct preheated the incoming air, and the heater power-control unit was used to adjust the air temperature. A thermocouple (type K, 1 °C) embedded in the control component was used to monitor the temperature inside the drying chamber continuously. To reach higher temperatures, the air was routed through a series of electrical resistance heaters before being redirected to the drying chamber. The drying air is directed horizontally over the samples. To control air velocity, an axial flow blower and a module for controlling its rotation speed were used. The air velocity was measured using a digital hot wire anemometer (TESTO 425, 0.03 m/s, made in Germany). The airflow velocity varied between 1.2 and 4.2 m/s, and the air temperature varied between 45 and 75 °C. The air temperature and airflow velocity value ranges were chosen based on the available research literature on industrial air drying applications.

The dryer was left idle for about 30 min before each experiment to achieve a steady-state based on predetermined experimental drying conditions. The samples were then stacked uniformly in a thin layer on a perforated tray within the LSWDM in a specific mass. The moisture content (MC) reduction was measured regularly (every 5–40 h). As a result, the drying process was terminated once the MC of the samples reached an equilibrium moisture content (EMC). To eliminate experimental error, all drying experiments were performed in triplicate, and the mean value was then adopted.

### 2.4. Measurement of relevant drying parameters

The MC of the samples was carried out on a dry basis in accordance with the standard procedure documented by the American Society for Testing and Materials standard method (ASTM D2974-14). Equation (1) calculates the final MC at a given time. Similarly, Equations (2) and (3) are used to calculate the dimensionless moisture ratio (MR) and the water activity ($a_w$) value (which measure the extent to which inherent moisture content can be involved in physical and chemical deteriorative reactions).

$$\%MC = \frac{w_2}{w_1} * 100 \tag{1}$$

$$MR = \frac{M_t - M_e}{M_0 - M_e} \tag{2}$$

$$a_w = \frac{\%RH}{100} \tag{3}$$

Where $w_2$ and $w_1$ are the post and pre-drying weight of the MaW sample. RH is the relative humidity, while $M_t$, $M_o$, and $M_e$ are moisture contents (MC) at any instant of time, initial MC and equilibrium MC, respectively.

### 2.5. Mathematical modeling

The drying data from GmW and MaW were fitted into five (5) thin-layer drying models and five (5) moisture desorption isotherm models. The theoretical foundations of the models have been extensively discussed in the literature [15,26,27], and the mathematical expressions of the models are presented in Tables 1 and 2, respectively. The experimental data were modeled using the Microsoft Excel 2016 SOLVER function. The $R^2$ and SSE values were used to determine the goodness of the respective model fit [28]. state that the higher the $R^2$-values and the lower the SSE values, the better the model fitting. Equations (4) and (5) were used to calculate the $R^2$ and SSE values, respectively [29].

$$R^2 = \frac{\sum_{i=1}^{N}\left(MR_i - MR_{pre,i}\right).\sum_{i=1}^{N}\left(MR_i - MR_{exp,i}\right)}{\sqrt{\left[\sum_{i=1}^{N}\left(MR_i - MR_{pre,i}\right)^2\right].\left[\sum_{i=1}^{N}\left(MR_i - MR_{exp,i}\right)^2\right]}} \tag{4}$$

**Table 1**
Kinetics models adopted in the study.

| S/N | Model names | Model equation |
|---|---|---|
| 1 | Logarithmic [30] | $MR = a_L * \exp(-k_L t) + c_L$ |
| 2 | Parabolic [31] | $MR = a_P + b_P t + c_P t^2$ |
| 3 | Henderson-Pabis [32] | $MR = a_H * \exp(-k_H t)$ |
| 4 | Demir et al. [33] | $MR = a_D * \exp(-k_D t)^n + b_D$ |
| 5 | Midilli [15] | $MR = a_M * \exp(-k_M t) + b_M t$ |

MR = Moisture ratio.

**Table 2**
Moisture desorption isotherm models adopted in the study.

| S/N | Model | Model equation |
|---|---|---|
| 1 | BET [34] | $EMC = \frac{m_o * C_B * a_w}{(1-a_w)*(1-a_w+C_B a_w)}$ |
| 2 | GAB [35] | $EMC = \frac{x_m + k\frac{c_G}{T}a_w}{(1-k_G a_w)\left(1-k_G a_w+\frac{c_G}{T}k_G a_w\right)}$ |
| 3 | Henderson [36] | $EMC = \left(-\frac{ln(1-a_w)}{c_{He}}\right)\frac{1}{n}$ |
| 4 | Halsey [37] | $EMC = \left[-\frac{exp(A_{Ha}+B_{Ha}T)}{ln\, a_w}\right]\frac{1}{C}$ |
| 5 | Oswin [38] | $EMC = C_O\left[\frac{a_w}{1-a_w}\right]^n$ |

EMC = equilibrium moisture content; $a_w$ = experimentally derived water activity; and T = temperature.

$$SSE = \frac{1}{N}\sum_{i=1}^{N}\left(MR_i - MR_{pre}\right)^2 \quad (5)$$

Where $MR_{exp}$ is the experimentally derived moisture ratio, $MR_i$ is the ith value of the moisture ratio to be predicted, $MR_{pre}$ is the model predicted moisture ratio and N is the number of observations.

### 2.6. Determination of the thermodynamic parameters

The effective moisture diffusivity (Deff) of a given drying operation is required to calculate the relevant thermodynamic parameter. The effective moisture diffusivity is calculated using Fick's diffusion equation for particles with slab geometry. As a result, Fick's equation for describing effective moisture diffusivity is commonly written as Equation (6).

$$MR = \frac{M - M_e}{M_0 - M_e} = \frac{8}{\pi^2}\sum_{n-1}^{\infty}\frac{1}{(2n-1)^2}\exp\left(\frac{-D_{eff}(2n-1)^2\pi^2 t}{4L^2}\right) \quad (6)$$

Where 'n' is the number of terms taken into consideration, 't' is the drying time (s), '$D_{eff}$' is effective moisture diffusivity ($m^2/s$) and 'L' is the average thickness of the sample (m). After considering the first term of Equation (6) for a long drying period [39], reported a simplification of Equation (6) to Equation (7). Upon linearization, Equation (7) becomes Equation (8).

$$MR = \left(\frac{8}{\pi^2}\right)\exp\left(\frac{\pi^2 D_{eff} t}{4L^2}\right) \quad (7)$$

$$\ln(MR) = \ln\left(\frac{M - M_e}{M_0 - M_e}\right) = \ln\left(\frac{8}{\pi^2}\right) - \left(\frac{D_{eff}\pi^2 t}{4L^2}\right) \quad (8)$$

Furthermore, the activation energy ($E_a$) can be computed using the Arrhenius type equation expressed in Equation (9), whose linearization yields Equation (10).

$$D_{eff} = D_o \exp\left(-\frac{E_a}{RT}\right) \quad (9)$$

$$\ln(D_{eff}) = \ln(D_o) - \left(\frac{E_a}{R}\right)\left(\frac{1}{T}\right) \quad (10)$$

Where $E_a$ is the activation energy (kJ/mol), R is the universal gas constant (8.3143 kJ/mol. K), T is absolute air temperature (K), $D_o$ is the pre-exponential factor of the equation ($m^2/s$). The plot of ln ($D_{eff}$) against 1/T will give the $E_a$ and $D_o$ as the slope and intercept, respectively. After the determination of activation energy, the different thermodynamic properties such as enthalpy (ΔH), entropy (ΔS) and Gibbs free energy (ΔG) can be determined accordingly using Equations 11–13.

$$\Delta H = E_a - RT \quad (11)$$

$$\Delta S = R\left[Ink - In\left(\frac{k_b}{k_h}\right) - \ln T\right] \quad (12)$$

$$\Delta G = \Delta H - T\Delta S \quad (13)$$

Where $k_b$ and $k_h$ are Boltzmann ($m^2$ $kg.s^{-2}$ $K^{-1}$) and Planck's constant (J. s), respectively.

## 3. Results and discussion

### 3.1. Wood sample characterization

The characterization outcome expresses the physical properties and distinguishing characteristics of the GmW and MaW samples. GmW is a fast-growing wood specie and when freshly sawn, it has a medium-coarse texture, pale yellow color, and lustrous appearance. These findings are comparable to Roque et al., (2009). The MaW sample is slashing soft and has storied fibers. It also has a dull white appearance with brown streaks and a distinct sheath around the cell lumen.

The tissue dimensions of the selected wood species are shown in Table 3. The average lumen size of GmW and MaW is 147.44 μm and 99.22 μm, respectively. The lumen contains the majority of the water that will be dried in the wood. As a result, determining the size, nature, and arrangement of the lumen is required because it provides information on the amount of moisture content to be removed from the wood sample during drying.

A di-seriate ray width of solitary crystals is depicted in the MaW sample. The MaW sample has a fibre length, diameter, and bulk density of 1200 μm, 190 μm, and 730 kg/$m^3$, respectively, while the GmW sample has a fibre length, diameter, and bulk density of 790 μm, 165 μm, and 510 kg/$m^3$. MaW is suitable for heavy construction due to its small vessel and characteristic fine texture. The property descriptions of the GmW and MaW wood species agree with the findings of [40]; who stated that variations in fibre diameter, which is directly related to cell wall size and thickness, affect wood density.

Fig. 1(a) and (b) show photomicrographs of the wood rays of the tangential section of GmW and MaW woods. Understanding ray formation in wood anatomy is important because common wood drying defects have been shown to occur along with the rays. GmW wood has a multi-seriate ray arrangement, whereas MaW has a di-seriate arrangement. When GmW is not properly processed during drying, it is more prone to developing wood drying defects than di-seriate MaW.

Fig. 2(a) and (b) show photomicrographs of the lumen size of the transverse section of GmW and MaW. As a result, MaW with dense and multiple lumens with an average size of 99.22 μm will require fewer resources and skills to expel inherent free water than GmW with larger lumen sizes. The investigation of the anatomical features of the GmW and MaW samples reveals that wood species are distinct and distinctively different. As a result, it is safe to say that no two wood species have the same anatomical features and characteristics. This confirms the complex relationship and interactions between the parameters of the wood drying process.

### 3.2. Effect of process variables

#### 3.2.1. Effect of drying time on wood drying

The effect of drying time (h) on MC reduction (%) for GmW and MaW is shown in Fig. 3. The drying time varied by 5 h from 0 to 40 h, as shown in Fig. 3. GmW and MaW both had an initial MC of 90 % at 0 h. However, it was found that increasing the drying time from 0 to 30 h resulted in an increase in the percentage of moisture loss from the wood samples. A negligible MC reduction was observed after 30 h, implying that the EMC was achieved in all wood samples after 30 h of drying. Furthermore, rapid moisture loss was observed for the wood samples within the first 5 h of drying. For example, approximately 55 % of GmW and 71 % of MaW of MC were lost. According to Ref. [41]; free water held loosely in any wood sample will be easily lost during drying. As a result, the initial rapid loss of a relatively large amount of moisture for the wood samples could be attributed to the loss of available free waters held by very weak forces. The previously observed rapid MC loss was no longer present after drying for 10 h. In addition, only about 5.6 % and 6.06 % of MC GmW and MaW were lost, respectively. As expected, the percentage of moisture loss decreased as the drying time increased. This is because the MC that remained in the wood samples after the initial rapid loss of free waters is now increasingly strongly bound to the interior of the wood [41]. The %MC loss from the samples decreased further as the drying time exceeded 10 h. Because the %MC within the wood interior at this point is bound by very strong chemical bonds, only a minimal percentage moisture loss of 7.09 % for GmW and 8.03 % for MaW was recorded from 10 h to 30 h of drying, as shown in Fig. 3. As a result, even at a relatively high operating temperature of 70 °C, moisture escapes more slowly.

So far, it has been established that GmW and MaW showed a general trend of decreasing %MC loss as drying time increased. It should be noted, however, that the %MC loss from MaW was significantly higher than that of GmW at each time interval during the drying process. This could be attributed to the fact that, in contrast to GmW, which is resistant to excessive drought and rapid water loss due to its superior structural orientation, MaW, with its dense, small but multiple lumen size, is only slightly drought resistant and dries quickly [42].

**Table 3**
Tissue dimensions of selected wood species.

| S/N | Name of specie | Trade name | Lumen size (μm) | Fibre length (μm) | Fibre diameter (μm) | Density (kg/$m^3$) | Ray width |
|---|---|---|---|---|---|---|---|
| 1 | Gmelina Arborea (GmW) | Gmelina | 147.44 | 790 | 165 | 510 | Multi-seriate |
| 2 | Mansoniaaltissima (MaW) | Ofun/Mansonia | 99.22 | 1200 | 190 | 730 | Di-seriate |

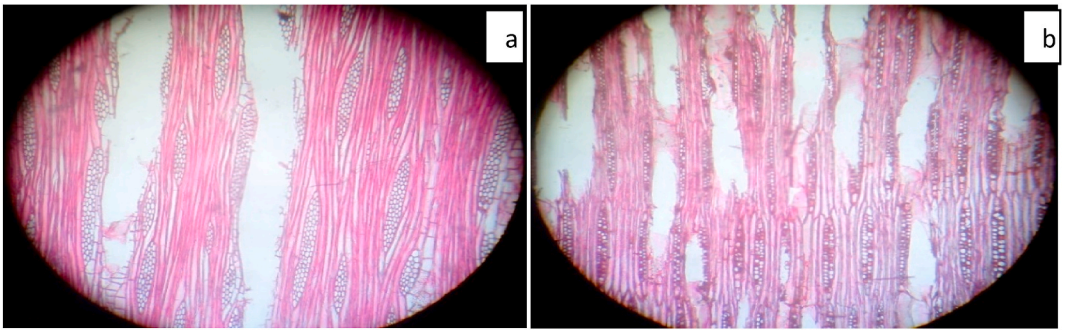


**Fig. 1.** Photomicrograph of the tangential section of the (a) GmW and (b) MaWsamples

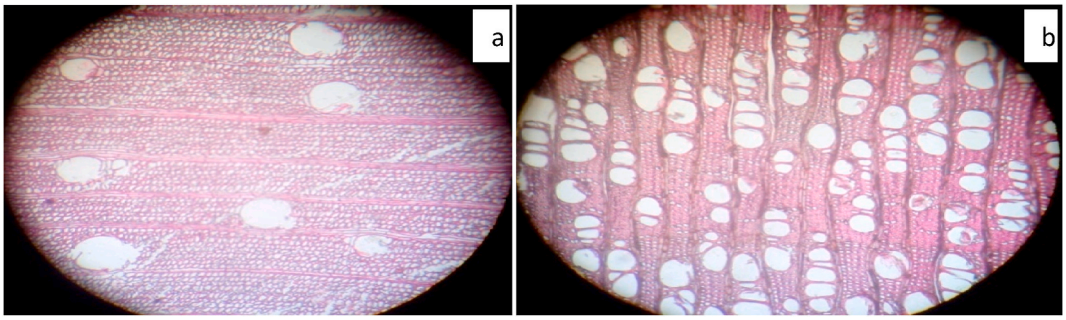


**Fig. 2.** Photomicrograph of the transverse section of the (a) GmW and (b) MaW samples.

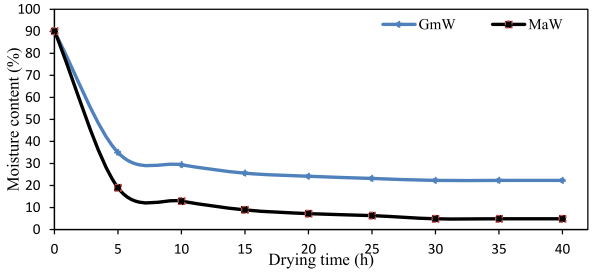


**Fig. 3.** Plot of the effect of drying time on moisture content reduction [Air velocity = 4.2 m/s, Temp = 70 °C].

### 3.2.2. *Effect of air velocity on wood drying*

Uniform air movement across the surface of moisture-laden material is required for efficient and effective drying [43]. This is due to the fact that effective airflow is important for two reasons: transferring heat energy sufficient to evaporate the moisture and transporting the vaporized moisture away from the wood surface. Fig. 4 depicts a graphical representation of the relationship between air velocity and %MC. This relationship must be established in order to determine the optimum air velocity for a given drying operation.

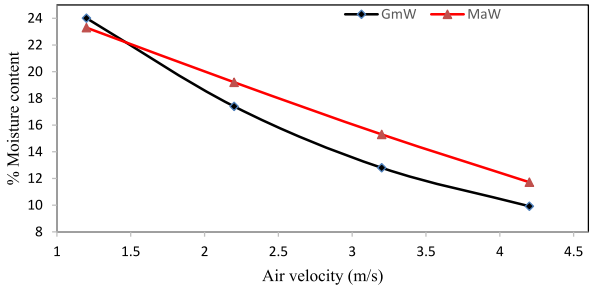


**Fig. 4.** Plot of the effect of air velocity on %moisture content [Time = 30 h, Temp = 70 °C].

At 90 % initial MC, air velocity in the range of 1.2–4.2 m/s was considered in this study. The graph generally depicted a consistent decrease in %MC for all samples as the air velocity was increased from 1.2 to 4.2 m/s at a maximum drying time of 30 h.

At an air velocity of 1.2 m/s, a final MC of 24.01 % (GmW) and 23.30 % (MaW) was recorded, resulting in a %MC loss of approximately 65.99 % (GmW) and 66.70 % (MaW). When the air velocity was increased to 2.2 m/s, the percentage moisture loss was 72.42 % (GmW) and 66.70 % (MaW). A comparison of the percentage moisture loss values revealed that a unit increase in air velocity from 1.2 to 2.2 m/s resulted in approximately 6.61 % (GmW) and 4.09 % (MaW) increase in the percentage moisture loss. By increasing the air velocity to 4.2 m/s, a similar increase in percentage moisture loss decrease in MC was observed for GmW and MaW, as shown in Fig. 4.

The low percentage moisture loss values were observed with a decrease in air velocity from 4.2 to 1.2 m/s could be explained. According to Ref. [43]; air movement across wet surfaces causes a drop in air temperature and a corresponding rise in air humidity. The volume of airflow determines the temperature drop and rise in relative humidity. As a result, at low air velocity, there is limited airflow across the wet surface, resulting in a rapid rise in relative humidity and a subsequent drop in air temperature. When this occurs, a low %MC loss is recorded, as observed correctly in the study. Similarly, increasing the air velocity from 1.2 to 4.2 m/s causes an increase in airflow volume through the sample's surface and interstitial space. This increase in airflow implies more airflow across the surface of the wood samples, resulting in a smaller temperature drop and a smaller rise in relative humidity. This explains why the %MC loss increased as air velocity increased.

#### 3.2.3. *Effect of temperature on wood drying*

Temperature is a critical factor that has a significant impact on the drying efficiency of any material. As a result, determining the maximum temperature for a given drying process is essential, as using an excessively high or low operational temperature may have a negative impact on the quality of the dried products. The effect of temperature was investigated in this study over a temperature range of 50–70 °C at an initial MC of 90 %. Fig. 5 depicts the graphical representation. The findings revealed that increasing the temperature resulted in a corresponding increase in the %MC loss decrease in MC from the wood samples.

The %MC recorded for GmW and MaW samples at 50 °C was 20.52 % and 19.20 %, respectively. These values translate to 69.48 % and 70.80 % MC loss for GmW and MaW, respectively. Similarly, the final %MC recorded for GmW and MaW samples at the upper drying temperature limit of 70 °C was 8.92 % and 7.20 %, respectively. These figures equate to 81.08 % moisture loss for GmW and 82.80 % moisture loss for MaW. Further investigation revealed that increasing the temperature by 20 °C from 50 to 70 °C resulted in a significant increase in %MC loss for the respective wood samples of 11.60 % for GmW and 12.00 % for MaW. It was also discovered that for every 5 °C increase in temperature, the %MC loss became less significant. For example, as the temperature increased from 50 °C to 55 °C., the percentage of moisture loss increased by 7 % on average across all wood samples. An increase in temperature from 55 to 60 °C and from 60 to 65 °C resulted in a 3 % and 1 % increase in percentage moisture loss, respectively, for all samples.

The probable reason for the observed trend of an experimental result is explained. At the molecular level, thermal energy is associated with directional motion, and when there is energy impact, moistures easily move to the wood surface where they are evaporated [43]. As a result, as the temperature rises from 50 to 70 °C, the water molecules in wood materials move faster and collide more violently. This violent collision greatly increases the likelihood of bond cleavages and rearrangements, allowing water molecules to escape from the wood samples. This statement confirms that heated water with higher kinetic energy is more likely to be absorbed into the air than stationary water molecules with lower kinetic energy [44].

### 3.3. *Drying process modeling*

#### 3.3.1. *Modeling of moisture desorption isotherm*

Because water mobility across the wood sample is determined by water activity (equilibrium relative humidity), the desorption isotherm expresses the lowest achievable MC at constant temperature and pressure [45]. Table 4 shows five (5) mathematical models used in this study to describe the desorption isotherms of GmW and MaW. As a result, the best isotherm model was chosen based on the $R^2$ (Equation (4)), and SSE values (Equation (5)). According to the values in Table 4, the $R^2$ values for all models were unity, making it difficult to choose the best-fit model. To avoid the anomaly and uncertainty associated with the $R^2$ value, the desorption isotherm models were examined further using the AAD and SSE values. Table 4 showed that the AAD and SSE values for all isotherm models for

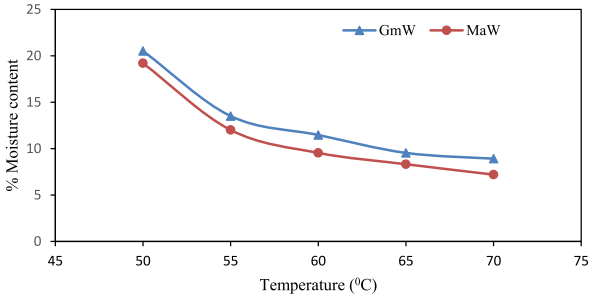


**Fig. 5.** Plot of the effect of temperature on % moisture content [Air velocity = 4.2 m/s, Time = 30 h].

the GmW and MaW samples were relatively large. Despite this anomaly, the model with the lowest AAD and SSE values will ultimately be the best-fit.

Although the recorded SSE values for GmW in Table 4 were relatively high for all models, the Oswin model had the lowest SSE value of 34.65. It is considered a good fit model for describing GmW moisture desorption. The average absolute deviation of 16.61 % for the Oswin model, on the other hand, is slightly higher than that of the Halsey model. Furthermore, the BET model emerged as the second best-fit model for GmW, with an SSE value of 20.51, which is approximately 6-fold higher than the Oswin model. However, its AAD value of 20.60 % is higher than Halsey's 16.28 %. This observation implies that Oswin and BET models depicted the lowest and second-lowest sum of the squared differences between each of their data points and the mean of the data set, respectively. Meanwhile, their average deviation from the corresponding experimental data points is greater than that of the Halsey model. It is well known that AAD outperforms SSE when determining the best-fit model, provided the observed errors are greater than unity. As a result, the Halsey model, with the lowest AAD value of 16.28 %, is considered the best-fit for GmW. The BET model with the lowest SSE values (SSE = 40.10) among the others is considered the best-fit for MaW. However, its AAD value of 21.97 % was slightly higher than Halsey's (20.91 %) and Oswin's (21.57 %). This observation implies that the BET model provided the smallest sum of squared differences between each of its data points and the data set mean. Meanwhile, the average deviation between its data points and the corresponding experimental data points is greater. Because AAD values outperform SSE values in terms of data prediction and analysis, the Halsey model with the lowest AAD value of 20.91 % is considered the best-fit for MaW, followed by the Oswin model.

Surprisingly, the Halsey model was found to be the best-fit model by maximization of $R^2$ values for GmW and MaW. As a result, it is possible to deduce the theoretical implications of the respective model's theoretical foundation on the current moisture desorption system. The Halsey and Oswin model expresses multilayer condensation at a relatively great distance from the surface. Its fundamental premise is that the potential energy of water molecules varies as the inverse of the nth power of their distance from the wood surface. With an increase in the thickness/layer of the desorbed moisture film, the potential energy differences are rapidly averaged. As a result, at less than a layer coverage, the system's energetic heterogeneities are irrelevant if the surface temperature is sufficiently high, leaving geometric heterogeneity as the primary moisture desorption factor. The experimentally determined equilibrium MC was compared with the predicted data sets generated by the various models, as shown in Fig. 6, to validate the established best-fit model. A strong correlation was found between the experimental data and the plotlines of the best fitting models, validating the best fitting performance.

### *3.3.2. Modeling of thin-layer drying kinetics*

Five (5) thin-layer models were used to investigate the thin-layer kinetics of MaW drying. The values of the goodness of fit models (Go-FMs), namely $R^2$, AAD, and SSE, were used to determine the models' consistency and fitting adequacy. Table 5 shows the model parameters and goodness of fit values generated by the non-linear regression method using the Microsoft Excel Solver add-in function. It was discovered that the $R^2$ values for the various kinetic models were all one (maximum value) for GmW and MaW. As a result, the best-fit model may be indistinguishable based on the $R^2$ value. Because of the uncertainty in the $R^2$ value description for the various models, the SSE and AAD values will be used instead. Table 5 showed that all of the isotherm models for the GmW and MaW samples had relatively small SSE values (less than 0.1 in all cases) and AAD values in the range of about 7–100 %.

Among the generally low SSE values recorded for all models for GmW, the Logarithmic model had the lowest SSE value of 9.0E-04. As a result, with an average absolute deviation of 16.08 %, is considered the best-fit model for describing the GmW moisture desorption. The emergence of the Logarithmic model as the best-fit does not imply that the remaining models are incapable of fitting. Based on their extremely low SSE values, all of the other models provided a reasonable description of the experimental data. Despite the fact that the other models had low SSE values, their AAD values varied greatly. The implication is that while the sum of squared differences between each observation and its group's mean is insignificant, the average of the absolute deviations from the experimental data set was very significant. The experimental moisture ratio values were compared with the predicted data sets generated by the different models, as shown in Fig. 7, to validate the established best-fit model. Demir et al., (2007) is a semi-theoretical thin-layer drying model that assumes the water molecules on the wood sample are homogeneous and isotropic, with constant effective moisture

**Table 4**
Isotherm parameter and corresponding goodness-of-fit test values obtained via maximization of $R^2$.

| BET | GAB | Henderson | Halsey | Oswin |
|---|---|---|---|---|
| GmW | | | | |
| $M_0 = 30.543$ | $k_G = 0.30$ | $C_H = 0.05$ | $A = 0.10$ | $C_O = 55.10$ |
| $C_B = 15.681$ | $x_G = 12.79$ | $n_H = 0.06$ | $B = 1.0E\text{-}04$ | $n_O = 0.47$ |
| $R^2 = 1.00$ | $C_G = 0.20$ | $R^2 = 1.00$ | $C = 0.02$ | $R^2 = 1.00$ |
| $SSE = 40.505$ | $R^2 = 1.00$ | $SSE = 55.29$ | $R^2 = 1.00$ | $SSE = 34.65$ |
| % AAD = 20.599 | $SSE = 87.54$ | % AAD = 27.37 | $SSE = 42.41$ | % AAD = 16.61 |
| | % AAD = 26.40 | | % AAD = 16.28 | |
| **MaW** | | | | |
| $M_0 = 28.13$ | $k_G = 0.30$ | $C_H = 0.06$ | $A = 1.03$ | $C_O = 25.08$ |
| $C_B = 14.47$ | $x_G = 11.25$ | $n_H = 0.07$ | $B = 1.0E\text{-}03$ | $n_O = 0.25$ |
| $R^2 = 1.00$ | $C_G = 0.20$ | $R^2 = 1.00$ | $C = 0.08$ | $R^2 = 1.00$ |
| $SSE = 40.09$ | $R^2 = 1.00$ | $SSE = 45.41$ | $R^2 = 1.00$ | $SSE = 53.87$ |
| % AAD = 21.97 | $SSE = 91.68$ | % AAD = 28.76 | $SSE = 51.30$ | % AAD = 21.57 |
| | % AAD = 31.44 | | % AAD = 20.91 | |

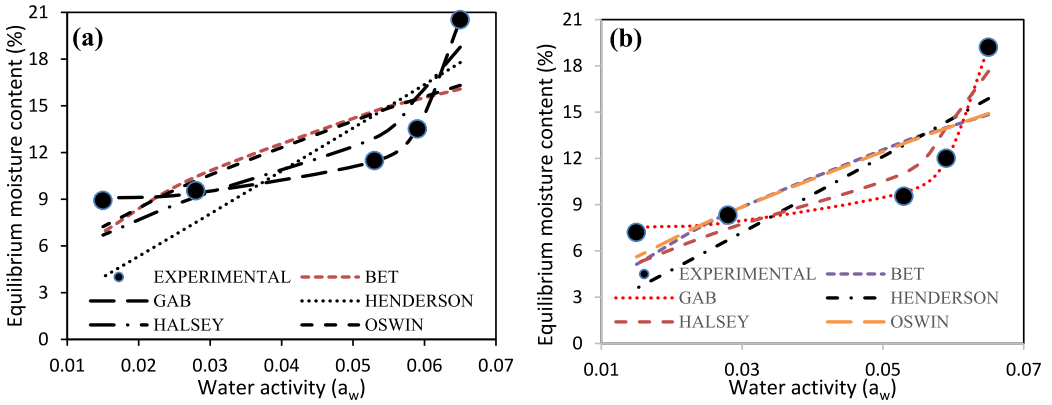


**Fig. 6.** The moisture desorption isotherm plot for (a) GmW and (b) MaW.

**Table 5**
Kinetic parameter and corresponding goodness-of-fit test values obtained via maximization of $R.^2$.

| Henderson-Pabis | Midilli-Kucuk | Logarithmic | Demir et al. | Parabolic |
|---|---|---|---|---|
| GmW | | | | |
| $a_H = 1.10$ | $a_M = 2.00$ | $a_L = 0.51$ | $a_D = 0.44$ | $a_P = 0.01$ |
| $k_H = 0.27$ | $b_M = 1.9E\text{-}03$ | $k_L = 0.19$ | $b_D = 0.03$ | $b_P = 0.01$ |
| $R^2 = 1.00$ | $K_M = 0.50$ | $c_L = 0.01$ | $k_D = 0.47$ | $c_P = -3.0E\text{-}04$ |
| SSE = 1.1E-02 | $R^2 = 1.00$ | $R^2 = 1.00$ | $n_D = 0.47$ | $R^2 = 1.0$ |
| % AAD = 63.08 | SSE = 7.0E-03 | SSE = 9.0E-04 | $R^2 = 1.00$ | SSE = 0.026 |
| | % AAD = 83.12 | % AAD = 16.08 | SSE = 1.5E-03 | % AAD = 146.22 |
| | | | % AAD = 38.80 | |
| MaW | | | | |
| $a_H = 1.15$ | $a_M = 2.00$ | $a_L = 0.50$ | $a_D = 0.44$ | $a_P = 0.01$ |
| $k_H = 0.29$ | $b_M = 1.6E\text{-}03$ | $k_L = 0.20$ | $b_D = 0.023$ | $b_P = 0.01$ |
| $R^2 = 1.00$ | $K_M = 0.49$ | $c_L = 0.01$ | $k_D = 0.47$ | $c_P = -3.3E\text{-}04$ |
| SSE = 0.01 | $R^2 = 1.00$ | $R^2 = 1.00$ | $n_D = 0.47$ | $R^2 = 1.00$ |
| % AAD = 69.51 | SSE = 5.2E-03 | SSE = 1.3E-03 | $R^2 = 1.00$ | SSE = 0.018 |
| | % AAD = 55.80 | % AAD = 22.30 | SSE = 7.4E-04 | % AAD = 110.58 |
| | | | % AAD = 19.26 | |

diffusivity, based on the theoretical background of the best-fit model [46]. Similarly, the models propose that the initial moisture content is unaffected by other parameters and that moisture equilibrium occurs at the wood surface. Furthermore, internal and external heat transfer is thought to be solely the result of conduction and convection, respectively.

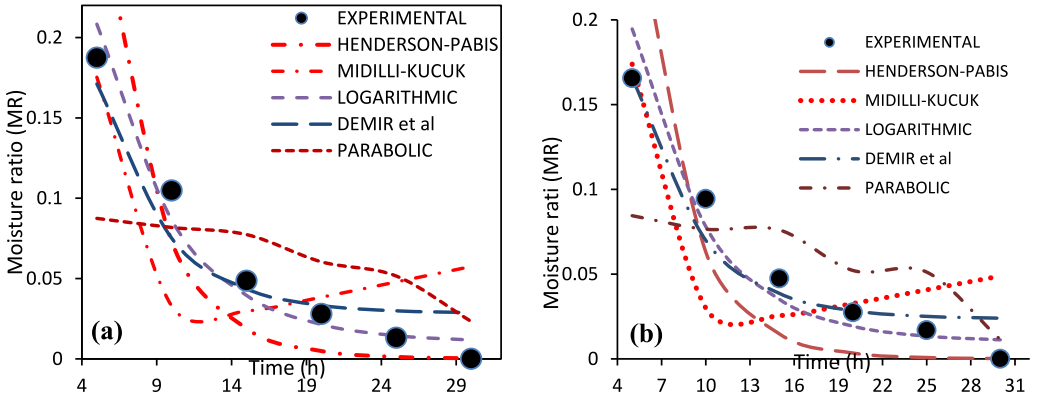


**Fig. 7.** Thin-layer kinetic model plots for (a) GmW and (b) MaW.

### 3.4. Thermodynamics modeling

Table 6 shows the enthalpy change (ΔH), entropy change (ΔS), and Gibbs free energy (ΔG) values of GmW and MaW calculated from desorption data. The ΔH value, which expresses the water-wood bond strength, was negative for the GmW and MaW samples at all temperatures, according to the data. The ΔH became increasingly negative as the temperature increased from 323 to 343 K. In theory, negative ΔH values are expected because the breakage of the intermolecular bond between the water molecules and the wood, as well as the subsequent diffusion of those water molecules to the drying surface, requires sufficient energy. Furthermore, the progressive decrease in ΔH values suggests that as the temperature rises, the energy required for the drying process decreases [47].

Table 6 shows that the entropy change (ΔS) values were negative and varied linearly with temperature. The negativity of the ΔS values increased with increasing temperature, following the same trend as the ΔH values. The presence of chemical desorption and/or structural alterations in the sample results in a negative ΔS value; thus, the drying process is considered entropically unfavorable [48]. Furthermore [49], believe that the inverse relationship between ΔS-values and temperature is due to the restriction of water molecule movement caused by significant moisture loss during drying.

The Gibbs free energy (ΔG) values were positive, indicating that the drying process was not spontaneous, and thus an external energy supply was required to facilitate the drying. This finding is consistent with [50]; who stated that drying is a non-spontaneous process. Furthermore, the magnitude of the ΔG values was 105 kJ/mol which is attributed to the work required to create available desorption sites. These values imply that significant effort was expended in developing active desorption sites on the GmW and MaW samples.

### 3.5. Effective diffusivity ($D_{eff}$)

The effective moisture diffusivity (Deff) describes the rate of moisture movement regardless of the mechanism at work [19,51]. The Deff values were calculated as the slope of the Ln (MR) versus drying time (s) plot for GmW and MaW, as shown in Fig. 8 and presented in Table 7. Visual inspection revealed that the Deff values increase linearly with temperature. Surprisingly, this slight decrease in Deff values persisted throughout the temperature range studied. Meanwhile [52], reported that the Deff value for agricultural products is typically in the $10^{-11}$ to $10^{-8}$ $m^2/s$ range. The Deff values recorded in the study, on the other hand, ranged from 2.9E-08 to 4.8E-08, which is consistent with past findings.

Further examination of Table 7 revealed that GmW has the highest Deff-value at lower temperatures (323–328 K), whereas MaW has the lowest Deff-value at lower (323–328 K) and higher (338–343 K) drying temperatures but has the greatest Deff variation at such temperatures. Increased drying temperature above ambient reduces the viscosity of the water in the wood samples and promotes its escape from the wood, resulting in the high Deff values measured at 323 K. However, as the temperature rises, the diffusion rate of water molecules away from the wood slows, resulting in the observed decrease in Deff-values due to the limited presence of water molecules in the drying process (Madamba et al., 1996). The coefficients obtained in this study support the findings of [53].

### 3.6. Activation energy ($E_a$)

The activation energy is the minimum amount of energy required to start a specific process [54]. Fig. 9 depicts the temperature-dependent variation of the effective moisture diffusivity (Deff) of GmW and MaW. The activation energy was calculated using the slope of the plot of ln (Deff) against 1/T. (Ea). Table 7 shows the Ea values obtained for GmW and MaW samples. The lower this value, the easier it is to start the diffusion process in the GmW and MaW samples. The Ea values obtained in the study were 252.7 kJ/mol for GmW and 313.6 kJ/mol for MaW, respectively. Table 7 shows that for the same drying treatment, the MaW had higher activation energy and pre-exponential factor (Do) values than the others. This occurrence could be explained by the greater variation in Deff values with temperature depicted by MaW. The activation energy followed the same trend as the pre-exponential factor, representing diffusivity as temperature increases toward infinity.

The magnitudes of Ea-values for agricultural and food products generally range from 12 kJ/mol to 110 kJ/mol, but those for hardwood may be higher, according to Ref. [22]. The obtained results revealed that, as expected, the Ea-values for GmW and MaW

**Table 6**
Thermodynamic properties showing the ΔH, ΔS and ΔG of the drying process.

| Sample | Temp (K) | +ΔG (kJ/mol) | -ΔH (kJ/mol) | -ΔS (J/mol*K) |
|---|---|---|---|---|
| **GmW** | 323 | 105437.0 | 2432.72 | 333.962 |
| | 328 | 107107.1 | 2474.29 | 334.090 |
| | 333 | 108777.9 | 2515.86 | 334.215 |
| | 338 | 110449.3 | 2557.43 | 334.339 |
| | 343 | 112121.3 | 2599.00 | 334.461 |
| **MaW** | 323 | 101913.5 | 2371.82 | 322.865 |
| | 328 | 103528.2 | 2413.39 | 322.993 |
| | 333 | 105143.4 | 2454.96 | 323.118 |
| | 338 | 106759.3 | 2496.53 | 323.242 |
| | 343 | 108375.9 | 2538.10 | 323.364 |

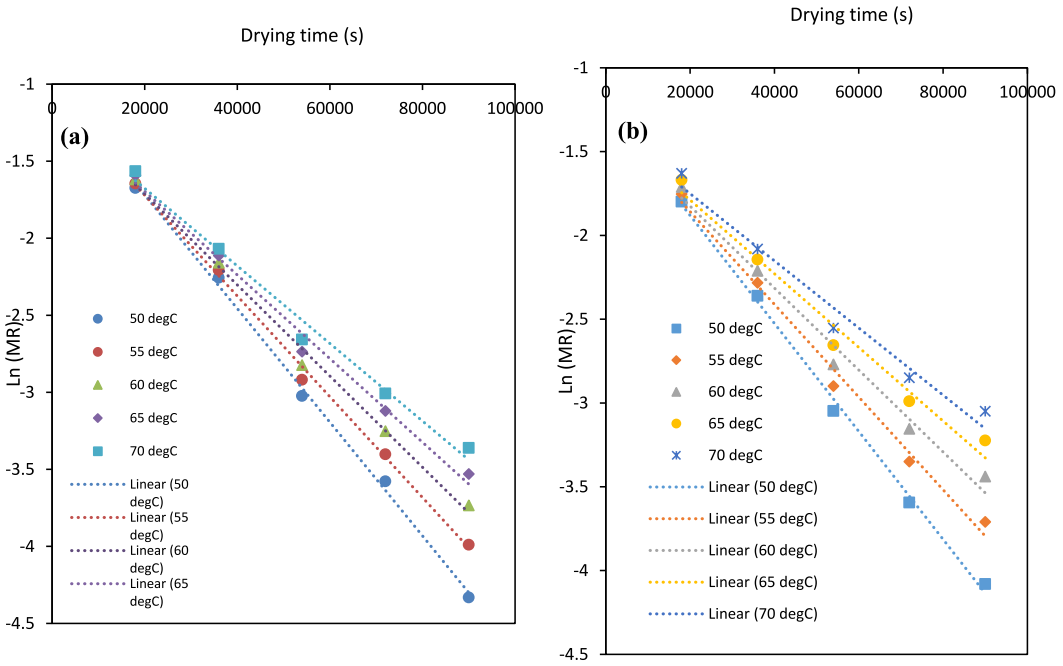


**Fig. 8.** Plots of Ln (MR) against t (s) for (a) GmW and (b) MaW.

**Table 7**
Thermodynamic parameters showing $E_a$ and $D_o$.

| Sample | Temp (K) | +$E_a$ (kJ/mol) | +$D_o$ ($m^2$/s) | $D_{eff}$ ($m^2$/s) |
|---|---|---|---|---|
| **GmW** | 323 | | | 5.378E-08 |
| | 328 | | | 4.769E-08 |
| | 333 | 252.702 | 2.41E-05 | 4.315E-08 |
| | 338 | | | 3.959E-08 |
| | 343 | | | 3.671E-08 |
| **MaW** | 323 | | | 4.678E-08 |
| | 328 | | | 4.034E-08 |
| | 333 | 313.604 | 9.17E-05 | 3.565E-08 |
| | 338 | | | 3.205E-08 |
| | 343 | | | 2.923E-08 |

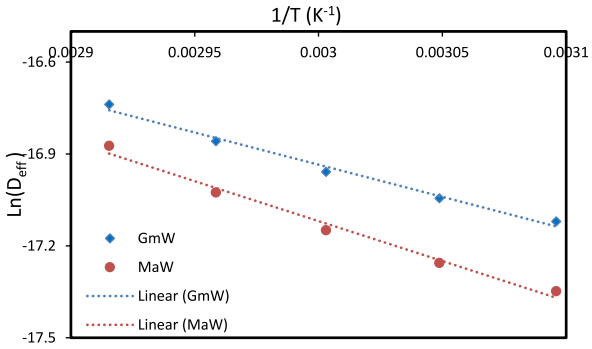


**Fig. 9.** The plot of Ln ($D_{eff}$) against 1/T ($K^{-1}$).

were higher than those reported by Ref. [22]. [54] also discovered two types of water in agricultural material: free and bounded water. Free water requires the least amount of Ea to escape compared to bounded water. The high Ea-values found in this study indicate that the majority of the inherent water in the GmW and MaW samples is bounded, implying a falling rate drying process.

## 4. Conclusion

The drying process parameters of GmW and MaW were modeled in this study using various thin layer and moisture desorption isotherm models. Investigating the samples' anatomical features reveals their distinct interior composition and confirms the complex relationship and interactions observed during the drying process. When the effects of the process variables were evaluated, it was found that the rate of moisture loss decreased as the drying time increased, with the optimum drying time being 30 h for the specified conditions. Furthermore, a consistent decrease in %MC was observed as air velocity increased from 1.2 to 4.2 m/s, whereas an increase in temperature resulted in a corresponding increase in %MC loss. The Halsey model was found to be the best-fit model for describing the moisture desorption isotherm for GmW and MaW based on the $R^2$ approach, while the GAB model was found to be the best-fit for the experimental desorption data for GmW and MaW. The Logarithmic model was deemed to be the best-fit model for describing the GmW, whereas the Demir et al. model demonstrated the best model behavior for the MaW. The presence of positive $\Delta G$ values indicates that the drying process is not spontaneous. The study also found a linear decrease in the effective diffusivity (Deff) values of the GmW and MaW samples as temperature increased, while the activation energy (Ea) values obtained were 252.7 kJ/mol for GmW and 313.6 kJ/mol for MaW. Prediction of the drying kinetics and moisture desorption isotherm of GmW and MaW was established while thermodynamic properties required for the effective and sustainable drying of GmW and MaW was determined. Overall, the process modeling and simulation of GmW and MaW wood drying can be used to identify the optimum drying conditions for these species. This research can be beneficial to wood processors who are looking to maximize the drying efficiency and quality of GmW and MaW wood.

## Data availability statement

No data was used for the research described in the article.

## Author contributions

Ugochukwu Okonkwo: Conceptualization, Formal analysis, Investigation, Supervision. Samuel Enibe: Conceptualization, Formal analysis, Methodology, Supervision. Chinagorom Ajike: Conceptualization, Formal analysis, Investigation, Methodology, Writing – original draft. Jeremiah Chukwuneke: Conceptualization, Formal analysis, Investigation, Methodology, Software, Validation, Writing – original draft, Writing – review & editing

## Declaration of competing interest

The authors declare that they have no known competing financial interests or personal relationships that could have appeared to influence the work reported in this paper.

## References

[1] O. Rotowa, E. Adekunle, A. Adeagbo, O. Nwanze, O. Fasiku, Economic analysis of agriculture, forestry and fisheries to the economic development of Nigeria, Int. J. Web Eng. Technol. 6 (2019) 1–14.
[2] J. Osagie, L. Otoide, Colonial rule and industrialization in Esan, Benin Province, Nigeria: a case study of institutional adaptation, African Research Review 9 (1) (2015) 73, https://doi.org/10.4314/afrrev.v9i1.7.
[3] J.L. Chukwuneke, M.C. Ewulonu, I.C. Chukwujike, P.C. Okolie, Physico-chemical analysis of pyrolyzed bio-oil from swietenia macrophylla (mahogany) wood, Heliyon 5 (6) (2019) e01790, https://doi.org/10.1016/j.heliyon.2019.e01790.
[4] M.H. Ramage, H. Burridge, M. Busse-Wicher, G. Fereday, T. Reynolds, D.U. Shah, G. Wu, L. Yu, P. Fleming, D. Densley-Tingley, The wood from the trees: the use of timber in construction, Renew. Sustain. Energy Rev. 68 (2017) 333–359.
[5] N.N. Mohd Za'im, H. Mohd Yusop, W.N. Wan Ismail, Synthesis of water-repellent coating for polyester fabric, Emerging Science Journal 5 (5) (2021) 747–754, https://doi.org/10.28991/esj-2021-01309.
[6] J. Chukwuneke, J. Sinebe, D. Ugwuegbu, C. Agulonu, Production by pyrolysis and analysis of bio-oil from mahogany wood (swietenia macrophylla), Br. J. Appl. Sci. Technol. 17 (4) (2016) 1–9, https://doi.org/10.9734/bjast/2016/24551.
[7] C.O. Aniagor, M.C. Menkiti, Kinetics and mechanistic description of adsorptive uptake of crystal violet dye by lignified elephant grass complexed isolate, J. Environ. Chem. Eng. 6 (2) (2018) 2105–2118, https://doi.org/10.1016/j.jece.2018.01.070.
[8] W. Kurdthongmee, K. Suwannarat, C. Wattanapanich, A framework to estimate the key point within an object based on a deep learning object detection, HighTech and Innovation Journal 4 (1) (2023) 106–121, https://doi.org/10.28991/hij-2023-04-01-08.
[9] O.A. Aregbesola, B.S. Ogunsina, A.E. Sofolahan, N.N. Chime, Mathematical modeling of thin layer drying characteristics of dika (Irvingia gabonensis) nuts and kernels, Niger. Food J. 33 (1) (2015) 83–89, https://doi.org/10.1016/j.nifoj.2015.04.012.
[10] E. Tarigan, G. Prateepchaikul, R. Yamsaengsung, A. Sirichote, P. Tekasakul, Drying characteristics of unshelled kernels of candle nuts, J. Food Eng. 79 (3) (2007) 828–833, https://doi.org/10.1016/j.jfoodeng.2006.02.048.
[11] J.L. Chukwuneke, C.H. Achebe, P.C. Okolie, E.A. Okafor, The effect of variety and drying on the engineering properties of fermented ground cassava, Int. J. Swim. Kinet. 1 (5) (2013) 13–27.
[12] S. Hassan-Beygi, M. Aghbashlo, M. Kianmehr, J. Massah, Drying characteristics of walnut [Juglans regia L.] during convection drying, Int. Agrophys. 23 (2) (2009) 129–135.
[13] R. Rémond, J. Passard, P. Perré, The effect of temperature and moisture content on the mechanical behaviour of wood: a comprehensive model applied to drying and bending, Eur. J. Mech. Solid. 26 (3) (2007) 558–572, https://doi.org/10.1016/j.euromechsol.2006.09.008.
[14] A. Taheri-Garavand, S. Rafiee, A. Keyhani, Mathematical modeling of thin layer drying kinetics of tomato influence of air dryer conditions, Int Trans. J. Eng. Manage. Sci. Tech 2 (2011) 147–160.
[15] A. Midilli, H. Kucuk, Mathematical modeling of thin layer drying of pistachio by using solar energy, Energy Convers. Manag. 44 (7) (2003) 1111–1122, https://doi.org/10.1016/s0196-8904(02)00099-7.
[16] P.S. Kumar, M. Kanwat, V.K. Choudhary, Mathematical modeling and thin-layer drying kinetics of bamboo slices on convective tray drying at varying temperature, J. Food Process. Preserv. 37 (5) (2012) 914–923, https://doi.org/10.1111/j.1745-4549.2012.00725.x.

[17] A. Belghith, S. Azzouz, A. ElCafsi, Desorption isotherms and mathematical modeling of thin layer drying kinetics of tomato, Heat Mass Tran. 52 (3) (2015) 407–419, https://doi.org/10.1007/s00231-015-1560-0.

[18] İ. Ceylan, Determination of drying characteristics of timber by using artificial neural networks and mathematical models, Dry. Technol. 26 (12) (2008) 1469–1476, https://doi.org/10.1080/07373930802412132.

[19] R. Amiri Chayjan, M. Kaveh, S. Khayati, Modeling drying characteristics of hawthorn fruit under microwave-convective conditions, J. Food Process. Preserv. 39 (3) (2014) 239–253, https://doi.org/10.1111/jfpp.12226.

[20] U.E. Inyang, I.O. Oboh, B.R. Etuk, Kinetic models for drying techniques—food materials, Adv. Chem. Eng. Sci. 8 (2) (2018) 27–48, https://doi.org/10.4236/aces.2018.82003.

[21] R. Lima-Corrêa de Aquino Brito, M. dos Santos Andrade, M.F. da Silva, G.F. das, J.T. Freire, M. do C. Ferreira, Thin-layer and vibrofluidized drying of basil leaves (Ocimum basilicum L.): analysis of drying homogeneity and influence of drying conditions on the composition of essential oil and leaf colour, Journal of Applied Research on Medicinal and Aromatic Plants 7 (2017) 54–63, https://doi.org/10.1016/j.jarmap.2017.05.001.

[22] M.H. Sonmete, H.O. Mengeş, C. Ertekin, M.M. Özcan, Mathematical modeling of thin layer drying of carrot slices by forced convection, J. Food Meas. Char. 11 (2) (2016) 629–638, https://doi.org/10.1007/s11694-016-9432-y.

[23] B.D. Argo, S. Sandra, U. Ubaidillah, Mathematical modeling on the thin layer drying kinetics of cassava chips in a multipurpose convective-type tray dryer heated by a gas burner, J. Mech. Sci. Technol. 32 (7) (2018) 3427–3435, https://doi.org/10.1007/s12206-018-0646-2.

[24] B.D. Argo, U. Ubaidillah, Thin-layer drying of cassava chips in multipurpose convective tray dryer: energy and exergy analyses, J. Mech. Sci. Technol. 34 (1) (2020) 435–442, https://doi.org/10.1007/s12206-019-1242-9.

[25] L. Cooper, R.L. Walls, J. Elser, M.A. Gandolfo, D.W. Stevenson, B. Smith, J. Preece, B. Athreya, C.J. Mungall, S. Rensing, M. Hiss, D. Lang, R. Reski, T. Z. Berardini, D. Li, E. Huala, M. Schaeffer, N. Menda, E. Arnaud, P. Jaiswal, The plant ontology as a tool for comparative plant anatomy and genomic analyses, Plant Cell Physiol. 54 (2) (2012), https://doi.org/10.1093/pcp/pcs163 e1–e1.

[26] K.A. Maigalura, J. Suleiman, Moisture sorption isotherm characteristics of awara food, Fudma Journal of Sciences 4 (2) (2020) 620–626, https://doi.org/10.33003/fjs-2020-0402-247.

[27] A.N. Aviara, Moisture sorption isotherms and isotherm model performance evaluation for food and agricultural products, Sorption in 2020s, IntechOpen 143 (2020), https://doi.org/10.5772/intechopen.87996.

[28] Q. Shi, Y. Zheng, Y. Zhao, Mathematical modeling on thin-layer heat pump drying of yacon (Smallanthus sonchifolius) slices, Energy Convers. Manag. 71 (2013) 208–216, https://doi.org/10.1016/j.enconman.2013.03.032.

[29] T.S. Dinani, N. Hamdami, M. Shahedi, M. Havet, Mathematical modeling of hot air/electrohydrodynamic (EHD) drying kinetics of mushroom slices, Energy Convers. Manag. 86 (2014) 70–80, https://doi.org/10.1016/j.enconman.2014.05.010.

[30] P.K. Chandra, R.P. Singh, Numerical integration, in: Applied Numerical Methods for Food and Agricultural Engineers, CRC Press, 2017, pp. 105–124, https://doi.org/10.1201/9781315137650-3.

[31] T.A. Shittu, A.O. Raji, Thin layer drying of african breadfruit (treculia africana) seeds: modeling and rehydration capacity, Food Bioprocess Technol. 4 (2) (2008) 224–231, https://doi.org/10.1007/s11947-008-0161-z.

[32] S.M. Henderson, S. Pabis, Temperature effects on drying coefficients, J. Agric. Eng. Res. 6 (1961) 169–174.

[33] V. Demir, T. Gunhan, A.K. Yagcioglu, Mathematical modelling of convection drying of green table olives, Biosyst. Eng. 98 (1) (2007) 47–53, https://doi.org/10.1016/j.biosystemseng.2007.06.011.

[34] S. Brunauer, P.H. Emmett, E. Teller, Adsorption of gases in multimolecular layers, J. Am. Chem. Soc. 60 (2) (1938) 309–319, https://doi.org/10.1021/ja01269a023.

[35] E.A. Guggenheim, Applications of Statistical Mechanics, Clarendon Press, Oxford, 1966.

[36] S.M. Henderson, A basic concept of equilibrium moisture, Trans. ASAE (Am. Soc. Agric. Eng.) 33 (1954) 29–32.

[37] G. Halsey, Physical adsorptionon non-uniformsurfaces, Journal of Chemistry and Physics 16 (1948) 931–937.

[38] C.R. Oswin, The kinetics of package life. III. The isotherm, Journal of the Society of Chemical Industry 65 (12) (1946) 419–421, https://doi.org/10.1002/jctb.5000651216.

[39] R.P. Kingsly, R.K. Goyal, M.R. Manikantan, S.M. Ilyas, Effects of pretreatments and drying air temperature on drying behaviour of peach slice, Int. J. Food Sci. Technol. 42 (1) (2007) 65–69, https://doi.org/10.1111/j.1365-2621.2006.01210.x.

[40] A.L. Jacobsen, L. Agenbag, K.J. Esler, R.B. Pratt, F.W. Ewers, S.D. Davis, Wood density, biomechanics and anatomical traits correlate with water stress in 17 evergreen shrub species of the Mediterranean-type climate region of South Africa, J. Ecol. 95 (2007) 171–183.

[41] Ö. Gezici-Koç, S.J.F. Erich, H.P. Huinink, L.G.J. van der Ven, O.C.G. Adan, Bound and free water distribution in wood during water uptake and drying as measured by 1D magnetic resonance imaging, Cellulose 24 (2) (2016) 535–553, https://doi.org/10.1007/s10570-016-1173-x.

[42] B. Falemara, J. Owoyemi, B. Olufemi, Physical properties of ten selected indigenous wood species in akure, ondo state, Nigeria, Journal of Sustainable Environmental Management 4 (2012) 16–23.

[43] M. David, Pneumatic Conveying Design Guide, third ed., Elsevier, Germany, 2016.

[44] M.C. Ndukwu, Effect of drying temperature and drying air velocity on the drying rate and drying constant of cocoa bean, Agricultural Eng. Int.: the CIGR e-journal 11 (2009) 12.

[45] G. Scaratti, A. De Noni Júnior, H.J. José, R. de Fatima Peralta Muniz Moreira, 1,4-Dioxane removal from water and membrane fouling elimination using CuO-coated ceramic membrane coupled with ozone, Environ. Sci. Pollut. Control Ser. 27 (18) (2020) 22144–22154, https://doi.org/10.1007/s11356-019-07497-6.

[46] C.D. Chukwunonye, N.R. Nnaemeka, O.V. Chijioke, N.C. Obiora, Thin layer drying modelling for some selected Nigerian produce: a review, Am J Food Sci Nutr Res 3 (1) (2016) 1–15.

[47] G. H. H. de Oliveira, D.M.S. Aragão, A.P.L.R. Oliveira, M.G. de Silva, A.C.A. Gusmão, Modelagem e propriedades termodinâmicas na secagem de morangos, Braz. J. Food Technol. 18 (4) (2015) 314–321, https://doi.org/10.1590/1981-6723.5315.

[48] R. Moreira, F. Chenlo, M.D. Torres, N. Vallejo, Thermodynamic analysis of experimental sorption isotherms of loquat and quince fruits, J. Food Eng. 88 (4) (2008) 514–521, https://doi.org/10.1016/j.jfoodeng.2008.03.011.

[49] P.C. Corrêa, F.M. Botelho, G.H.H. Oliveira, A.L.D. Goneli, O. Resende, S.D.C. Campos, Mathematical modeling of the drying process of corn ears, Acta Sci. Agron. 33 (4) (2011), https://doi.org/10.4025/actasciagron.v33i4.7079.

[50] Y.N. Nkolo Meze'e, J. Noah Ngamveng, S. Bardet, Effect of enthalpy–entropy compensation during sorption of water vapour in tropical woods: the case of Bubinga (Guibourtia Tessmanii J. Léonard; G. Pellegriniana J.L.), Thermochim. Acta 468 (1–2) (2008) 1–5, https://doi.org/10.1016/j.tca.2007.11.002.

[51] A. Touil, S. Chemkhi, F. Zagrouba, Moisture diffusivity and shrinkage of fruit and cladode of opuntia ficus-indica during infrared drying, Journal of Food Processing (2014) 1–9, https://doi.org/10.1155/2014/175402, 2014.

[52] P.S. Madamba, R.H. Driscoll, K.A. Buckle, The thin-layer drying characteristics of garlic slices, J. Food Eng. 29 (1) (1996) 75–97, https://doi.org/10.1016/0260-8774(95)00062-3.

[53] K. Sacilik, A.K. Elicin, The thin layer drying characteristics of organic apple slices, J. Food Eng. 73 (3) (2006) 281–289, https://doi.org/10.1016/j.jfoodeng.2005.03.024.

[54] R. Amiri Chayjan, J. Amiri Parian, M. Esna-Ashari, Modeling of moisture diffusivity, activation energy and specific energy consumption of high moisture corn in a fixed and fluidized bed convective dryer, Spanish J. Agric. Res. 9 (1) (2011) 28, https://doi.org/10.5424/sjar/20110901-077-10.